Supplementary Information

The Nb-Ti-W-O system as safe high power anodes for Li-ion batteries

J. Michael Sieffert, Christopher J. Lang, Stephanie Bazylevych, Shipeng Jia and Eric McCalla*

Department of Chemistry, McGill University, Montreal, Canada

* Corresponding author: eric.mccalla@mcgill.ca

Experimental methods:

High-throughput approaches have been utilized for all synthesis and characterization herein. First, a sol–gel method was adopted for the synthesis to achieve samples in the pseudoternary, as described in detail in ref.[S1]. Specifically, the samples were made by first dispensing varying volumes of 0.8 M WO_3, titanium butoxide, and ammonium niobate oxalate hydrate into alumina cups. Citric acid (3 M) was then added as a chelating agent. These homogenous precursor solutions then underwent a gelation process by heating at 60 °C, 110 °C, and 200 °C under vacuum. The resulting gels were crushed then outfitted with an 8×8 aluminum smokestack to prevent sample cross-contamination and off-gassed at 400 °C for 6 h to remove nitrates and citrate bi-products formed in the gelation process. After lifting and removing the smokestack, the samples were further calcinated at 1000 °C for 3 h in ambient air (heating at a rate of 10 °C min^{-1} and cooling rate of 5 °C min^{-1}).

All samples were first characterized using high-throughput XRD. The XRD measurements were performed in the transmission mode using a Panalytical Empyrean diffractometer with a Mo target (60 kV, 40 mA) and GalaPIX area detector, with all scans obtained at room temperature. For Mo Kα radiation (λ = 0.70926 Å for $K_{\alpha 1}$), a scattering angle range of 4–30° was selected (this corresponds to approximately 10–70° for Cu radiation). For all samples, the main peak intensity

was well over 1000 counts for the 10 min scans, demonstrating that the data is suitable for Rietveld refinements. Typically the strongest peaks had intensities of about 2000 counts and the noise in the background is about 10 such that peaks that are 1% of the strongest peak are still easily distinguishable above the background, we therefore estimate this to be our sensitivity to secondary phases in this study. Each scan took <10 min and an entire batch of 64 samples took <10 h. For ease of comparison to the rest of the literature, all patterns shown herein have had the Mo-Kα2 peaks stripped, and scattering angles have been converted to those that would be obtained with Cu-Kα1 ($\lambda = 1.54051$ Å) as described in detail in ref. [S2].

After XRD, a portion of each sample was then utilized for electrochemical testing. Combinatorial cells with 8 × 8 samples as electrode materials were used to test electrochemical properties. as described in detail in refs. [S3,S4]. Firstly, a custom-designed printed circuit board (PCB, Optima Tech) with 64 Ni pads was used. To create the electrodes, a slurry comprising of approximately 11 wt% carbon black and 5 wt% of PVDF and 0.3 mg of active material was drop casted onto the PCB as described in refs. [S5,S6]. This yields a mass loading of approximately 2.5 mg/cm^2. The PCB and electrodes were then dried at 60 °C overnight to evaporate NMP. The assembly of the combinatorial cell was performed in an argon-filled glovebox. The electrolyte was 1 M LiPF$_6$ in 1:1 EC: DMC (SoulBrain MI). Li metal foil was used as the counter electrode with two Whatman GF/D glass microfiber separators. The cell was then sealed using a 3M double-sided sealing tape as described in ref. (Potts et. Al.). Cyclic voltammetry (CV) was performed with the voltage range 1.0 to 3.0 V $vs.$ Li/Li$^+$ at a variety of scan rates on a lab-built high-throughput electrochemical system which utilizes a quad voltage source (Keithley 213) and a Keithley 2750 multichannel voltmeter. 64 CVs were performed simultaneously. Electrochemical testing was also performed at 37 °C in a house designed temperature-controlled apparatus in order to test the materials at human

body temperature. Data were processed to extract average voltages, and specific capacities over the multiple cycles performed. For the cycling experiments, a single protocol was used for the extraction of the key electrochemical parameters as shown in ref. [S1].

SEM was performed at the McGill Facility for Electron Microscopy Research (FEMR) on a Hitachi SU-8000. SEM-EDX was performed at the same time using an Oxford Instruments XMax 80 mm^2 detector, and the presented data is an average of 5 points representing 5 separate particles. XPS measurements were done using a ThermoScientific K-Alpha spectrometer equipped with an Al Kα micro-focused monochromator. The XPS measurements were done at a pressure of $\lll \approx 10^{-7}$ mbar with an X-ray spot size of 400μm. The survey and high-resolution spectra were collected with a pass energy of 200 and 30 eV, respectively. Ex situ samples were transferred directly from the glovebox to the XPS instrument without any exposure to air.

Table S1. Stoichiometry of the 9 key compositions discussed throughout the main text. Oxygen content is calculated assuming Ti^{4+}, W^{6+}, Nb^{5+}.

Sample label	Stoichiometry
A1	$Nb_{0.475}W_{0.525}O_{2.763}$
A2	$Nb_{0.475}W_{0.375}Ti_{0.15}O_{2.613}$
A3	$Nb_{0.325}W_{0.6}Ti_{0.075}O_{2.73}$
B1	$Nb_{0.85}W_{0.15}Ti_{0.2}O_{2.575}$
B2	$Nb_{0.85}W_{0.1}Ti_{0.05}O_{2.525}$
B3	$Nb_{0.85}W_{0.075}Ti_{0.075}O_{2.5}$
B4	$Nb_{0.775}W_{0.15}Ti_{0.075}O_{2.538}$
C1	$Nb_{0.85}Ti_{0.15}O_{2.425}$
C2	$Nb_{0.6}W_{0.1}Ti_{0.3}O_{2.4}$

Table S2. Slope (b) of the logarithm of the current vs. the logarithm of the scan rate. A value of b=1 corresponds to purely capacitive behavior, while b=0.5 corresponds to typical battery behavior. In all cases, b is closer to 1 for the "rectangle" than the peak as one would expect as a capacitor will show purely rectangular CVs. The values for the slope at the peak current are between 0.7 – 0.88 showing transitional behavior with significant variation in the extent of battery-like behavior. In all cases, R^2 values are very near unity.

Sample	b at 1.4 V (R^2)	B at peak current (R^2)
A1	0.94 (0.9925)	0.81 (1.00)
A2	0.93 (0.9882)	0.88 (0.9997)
B1	1.00 (0.9916)	0.83 (0.9988)
B4	0.90 (0.9919)	0.82 (0.9985)
C1	0.83 (0.991)	0.70 (0.9987)
C2	0.82 (0.962)	0.80 (0.9982)

Tables S3. Compositional analysis for a phase A material showing both the composition dispensed and measured using SEM-EDX. The sample is slightly rich in Nb, though within the error usually associated with EDX.

Element	Dispensed fraction	Measured fraction
Ti	0.15	0.155691
Nb	0.475	0.514798
W	0.375	0.329511

Tables S4. Compositional analysis for a phase B material showing both the composition dispensed and measured using SEM-EDX. The sample is slightly rich in Nb, though within the error usually associated with EDX.

Element	Dispensed fraction	Measured fraction
Ti	0.1	0.080994
Nb	0.8	0.834651
W	0.1	0.084355

Table S5. Fitting parameters obtained from XPS data of both pristine and charged materials. The patterns and fits are in Figures S1 and S9. It should be noted that the binding energies (BE) for Nb are shifting in the 1V sample, the quantification of each oxidation states molar abundance (%) should therefore be considered approximate, nonetheless the pattern in Figure S1 clearly shows a high amount of $Nb^{3/4+}$. For all other BE values here, there is excellent agreement with the literature[S7-S11].

| Sample	Nb			W			Ti		
	Sample	BE	%	Sample	BE	%	Sample	BE	%
B4 Pristine	Nb^{5+}	207.6	97.1	W^{6+}	36.3	86.6	Ti^{4+}	459.6	100
	Nb^{4+}	205.9	2.9	W^{5+}	34.8	13.4	Ti^{3+}	N/A	0
	Nb^{3+}	N/A	0	W^{4+}	N/A	0			
	Sample	BE	%	Sample	BE	%	Sample	BE	%
A2 Pristine	Nb^{5+}	207.9	96.9	W^{6+}	36.3	91.2	Ti^{4+}	459.5	97.2
	Nb^{4+}	206.3	3.1	W^{5+}	34.9	8.8	Ti^{3+}	457.9	2.8
	Nb^{3+}	N/A	0	W^{4+}	N/A	0			
	Sample	BE	%	Sample	BE	%	Sample	BE	%
A2 Charged to 2V	Nb^{5+}	208.2	85.1	W^{6+}	36.5	71	Ti^{4+}	459.6	87.9
	Nb^{4+}	206.7	14.9	W^{5+}	34.7	29	Ti^{3+}	457.8	12.1
	Nb^{3+}	N/A	0	W^{4+}	N/A	0			
	Sample	BE	%	Sample	BE	%			
A2 Charged to 1V	Nb^{5+}	210.2	12.3	W^{6+}	36.5	29.7	Sample	BE	%
	Nb^{4+}	207.9	53.2	W^{5+}	34.9	30.4	Ti^{4+}	459.8	43.6
	Nb^{3+}	205.5	35.5	W^{4+}	33.5	39.8	Ti^{3+}	458.1	56.4
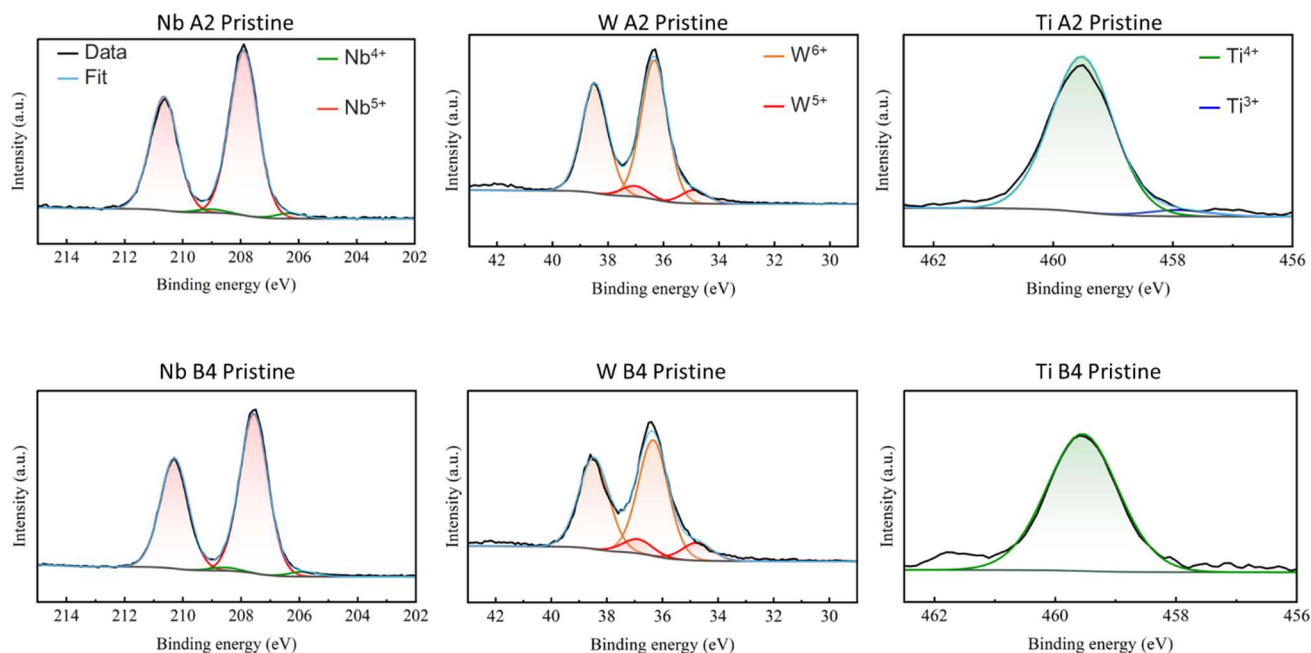
Figure S1: XPS results for the Nb 3d, W 4f and Ti 2p peaks for two pristine materials (A2 and B4). The results of the fitting are tabulated in Table S5 above. Though we report a small amount of Ti^{3+} in A2, it must be noted that this is barely above the background. By contrast, W^{5+} is well above the background and a poor fit is obtained without its inclusion.
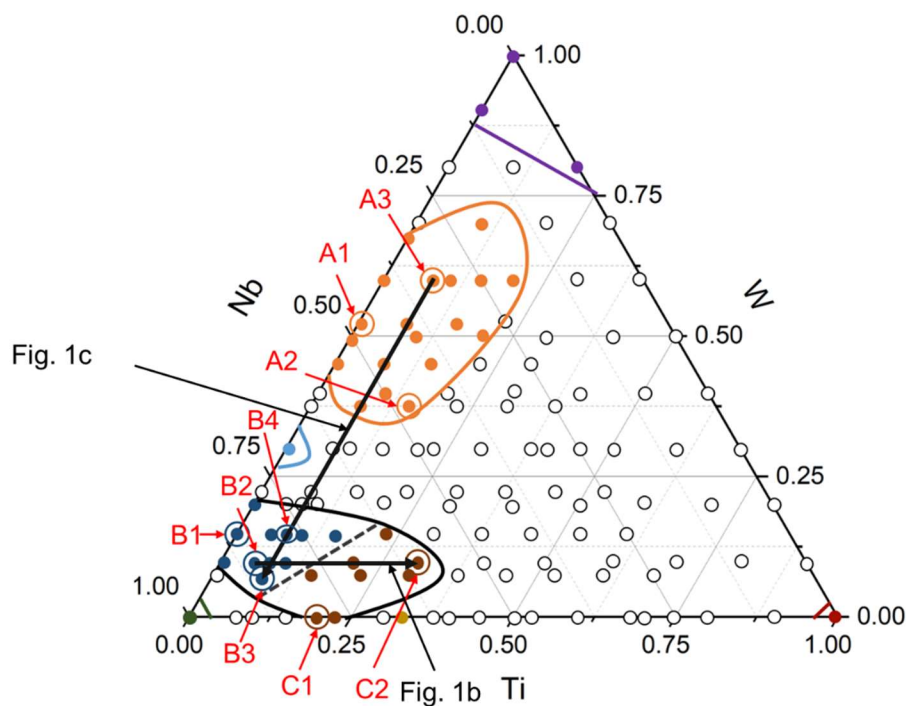
Figure S2: The $Nb_{1-x-y}Ti_xW_yO_z$ pseudoternary phase diagram showing the composition lines that are displayed in the XRD stacks in Figure 1b,c in the main text.
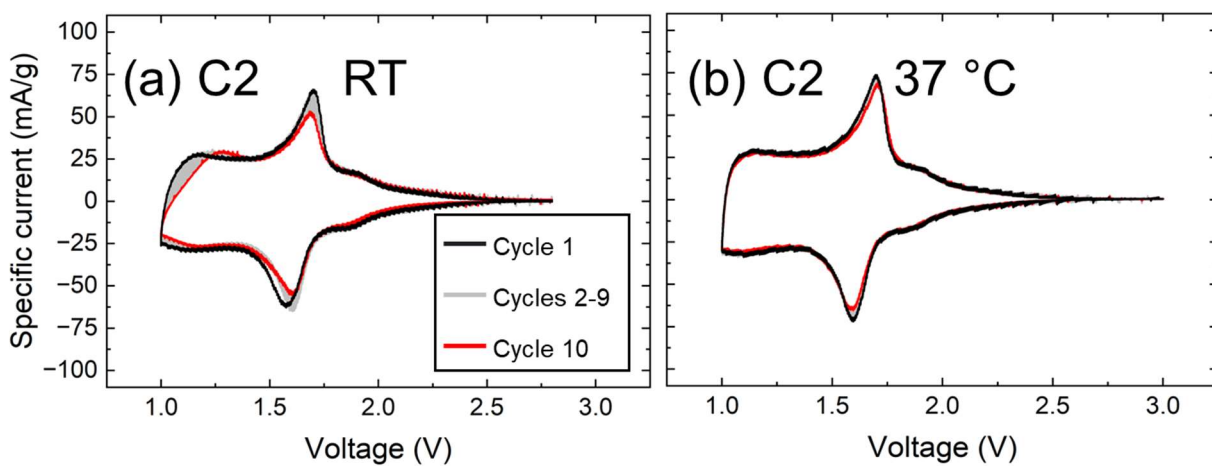
Figure S3: Cyclic voltammetry for materials C2 at RT (a) and 37 °C (b).
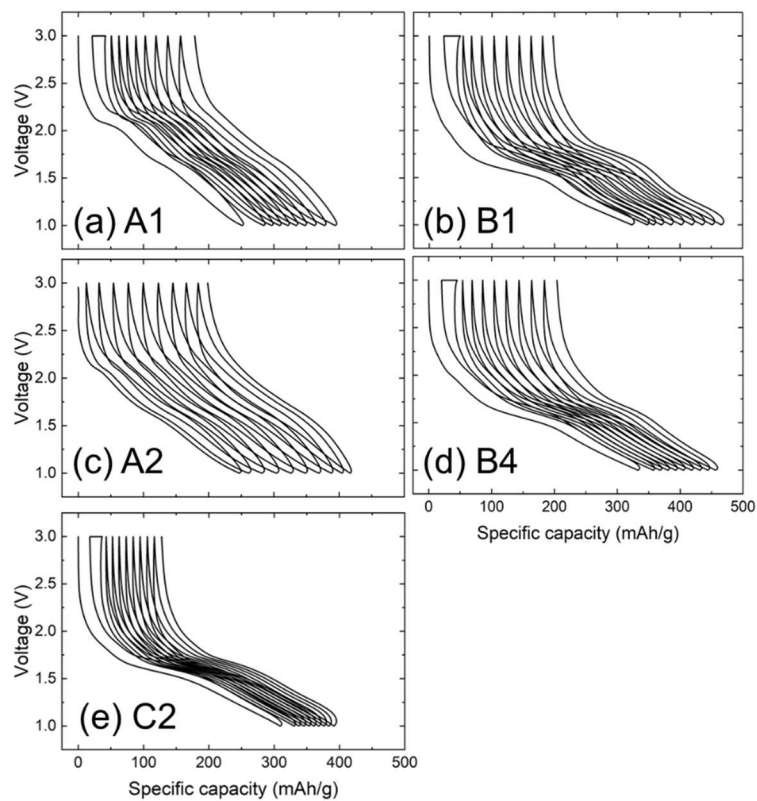
Figure S4: Voltage curves at RT for representative pseudoternary samples over 10 cycles at 0.1 V h^{-1} (0.0277 mV s^{-1}). Note that the extended cycling began with the 1st cycle and continued after the rate testing; the horizontal line seen here at 3V represents the plots skipping over the rate testing (not included here).
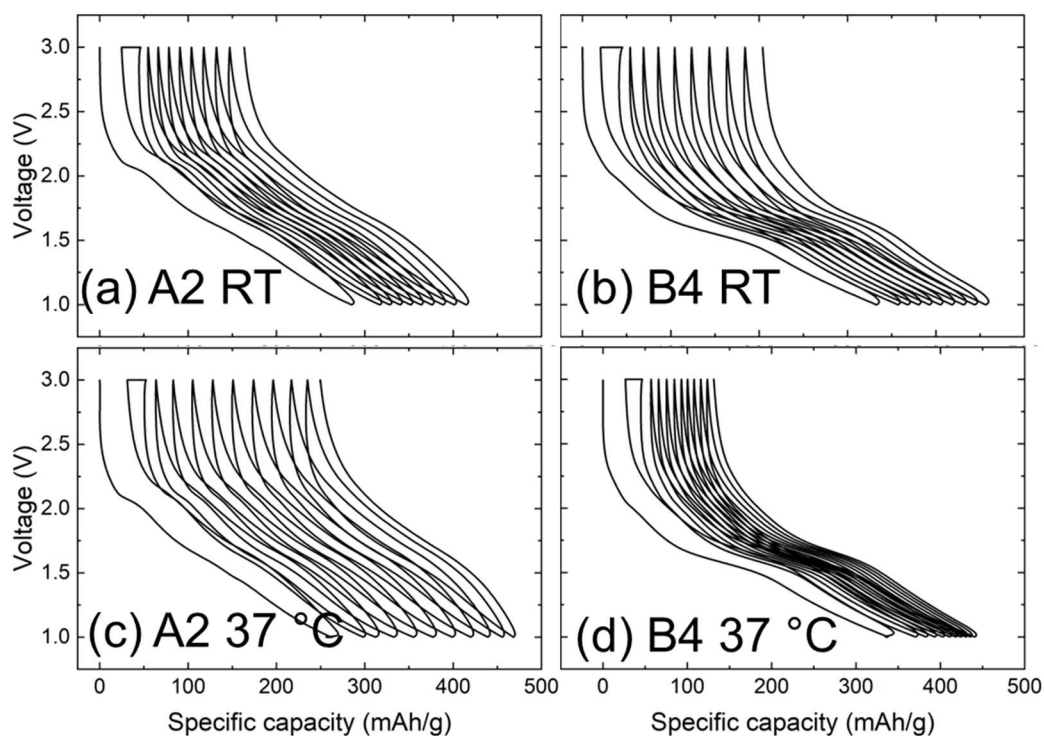
Figure S5: Voltage curves of sample A2 at (a) RT and (c) 37 °C and B4 at (b) RT and (d) 37 °C.
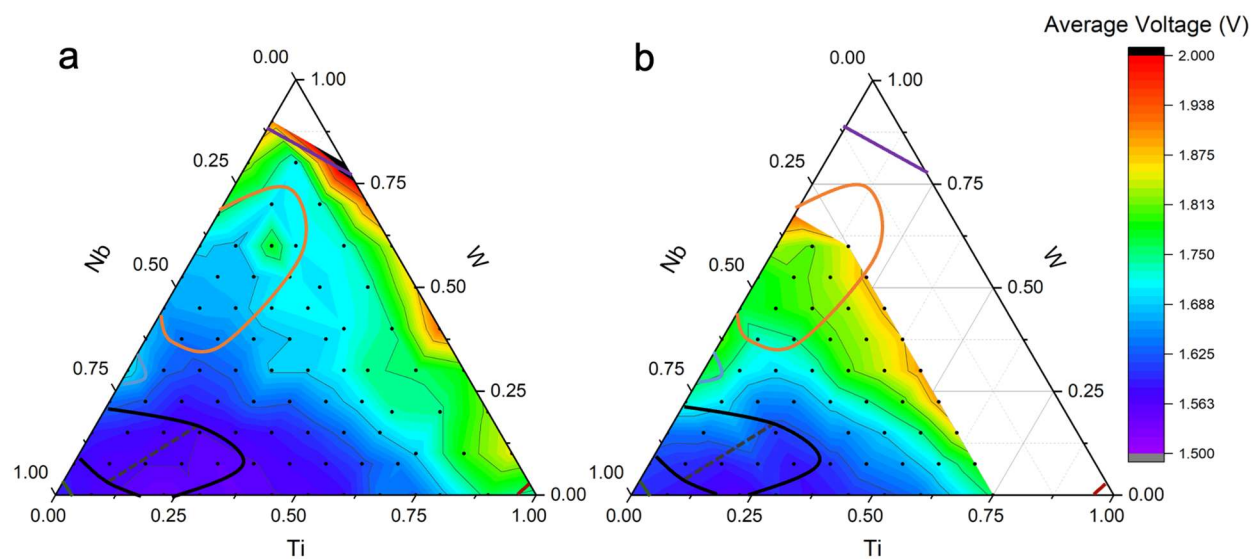

Figure S6: Average voltages of materials throughout the pseudoternary at (a) RT and (b) 37 °C. Since these are anodes, a low voltage will result in a higher voltage in a full cell and thus higher energy density.
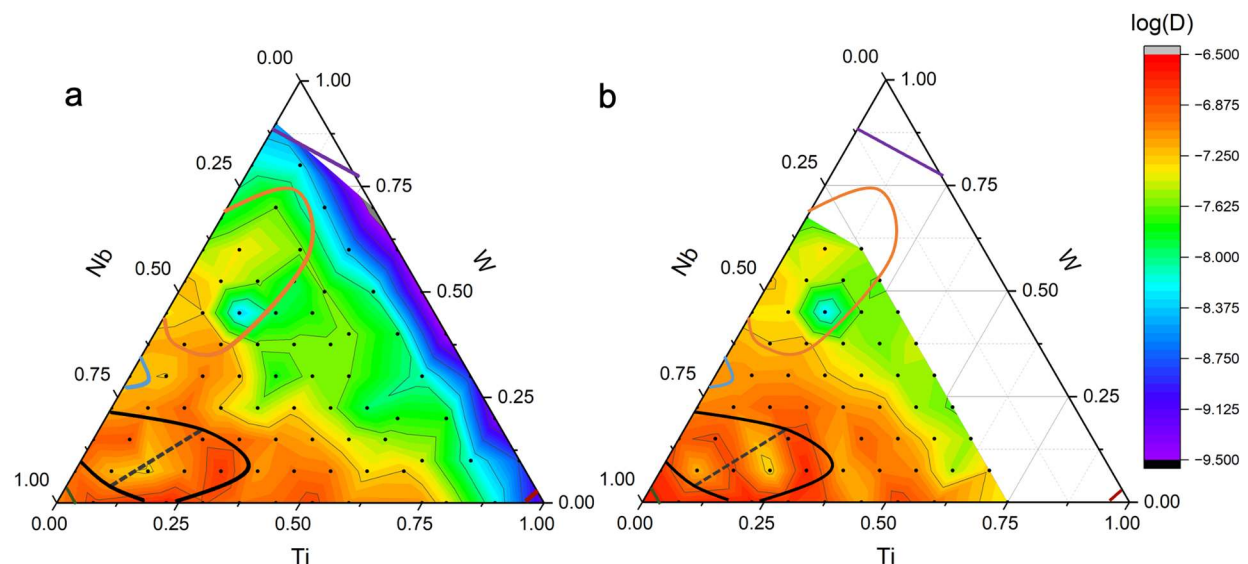
Figure S7: Logarithm of the chemical diffusion coefficient in cm^2 s^{-1} of the pseudoternary as derived by cyclic voltammetry at (a) RT and (b) 37 °C.
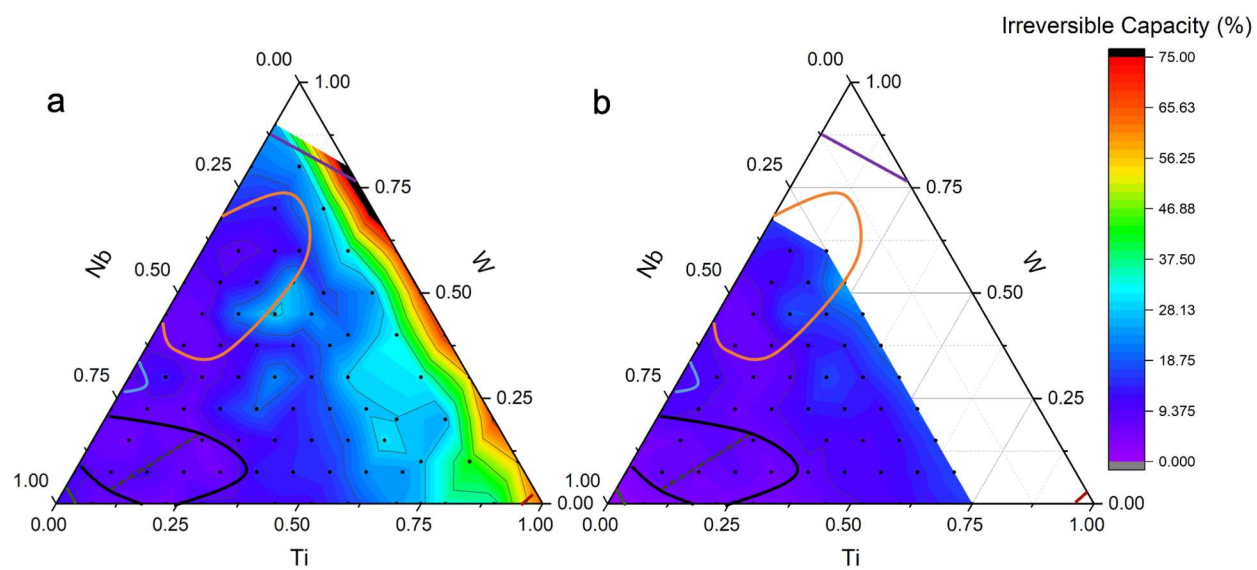

Figure S8: Irreversible 1st discharge capacity of the pseudoternary at (a) RT and (b) 37 °C.
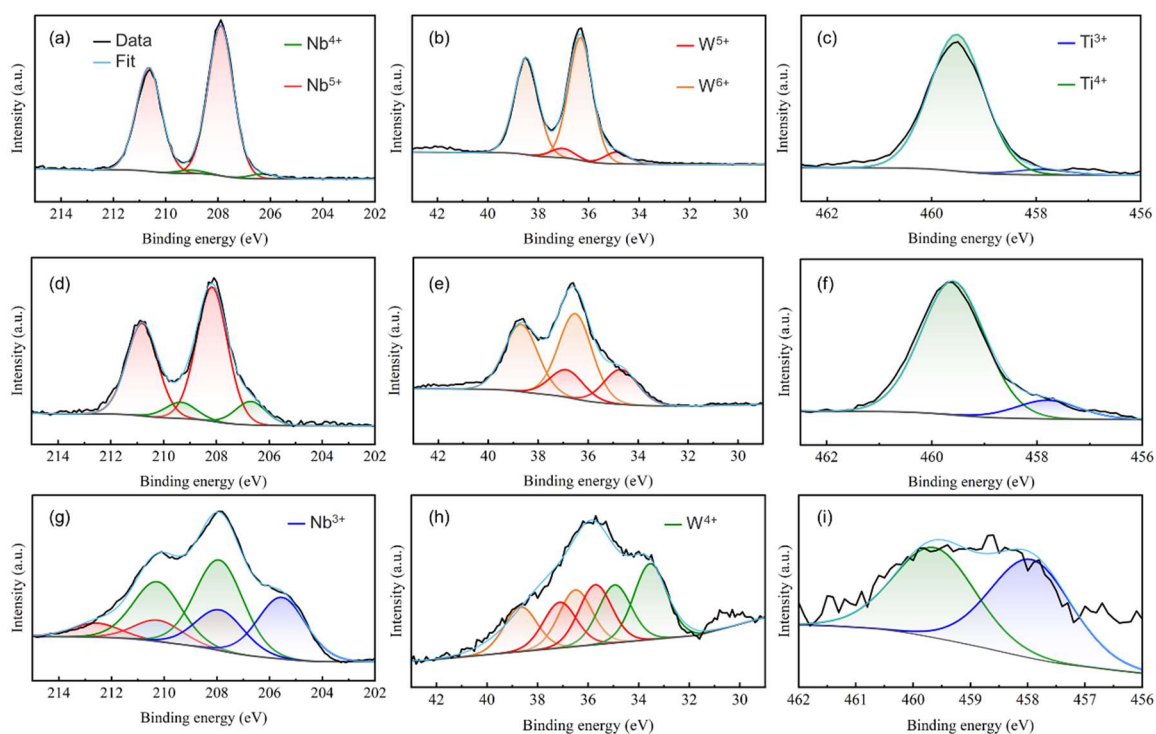
Figure S9: XPS results for the Nb 3d, W 4f and Ti 2p peaks for A2 materials: pristine (a,b,c), charged to 2 V (d,e,f) and charged to 1 V (g,h,i). The small amount of Ti makes the signal to noise poor, particularly in the ex situ 1 V sample, there is nonetheless enough signal near 458-460 eV to quantify the amount of Ti in the 3+ and 4+ states.The results of the fitting are tabulated in Table S5 above. Agreement with the literature is obtained for all fits (i.e. binding energies within 0.1 eV of the reported values in S7-S11), except g where signal in the range 213-214 eV results in shifting of the Nb^{5+} peaks and this in turn shifts the 4+ peaks, each by about 1 eV. The results of the fit in g are therefore considered approximate. However, it is unquestionable that a high portion of Nb is reduced to below 5+ with a significant amount in the 3+ state in this sample, this can be seen by comparing the raw data to those of the pristine and 2 V data.

References:

S1. Rehman, S.; Sieffert, J. M.; Lang, C. J.; McCalla, E. *$Nb_yW_{1-y}O_z$ and $Nb_xTi_{1-x}O_z$ pseudobinaries as anodes for Li-ion batteries*. Electrochimica Acta 2023, 439, 141665.

S2. McCalla, E.; Parmaklis, M.; Rehman, S.; Anderson, E.; Jia, S.; Hebert, A.; Potts, K.; Jonderian, A.; Adhikari, T.; Adamič, M. *Combinatorial methods in advanced battery materials design*. Canadian Journal of Chemistry 2022, 100, 132.

S3. Adhikari, T.; Hebert, A.; Adamič, M.; Yao, J.; Potts, K.; McCalla, E. *Development of high-throughput methods for sodium-ion battery cathodes*, ACS Combinatorial Science 22, 311–318 (2020).

S4. Potts, K.; Grignon, E.; McCalla, E. *Accelerated Screening of High Energy Li-Ion Battery Cathodes*, ACS Applied Energy Materials 2019, 2, 8388.

S5. Jonderian, A.; Jia, S.; Yoon, G.; Cozea, V.T.; Zeinali Galabi, N.; Ma, S.B.; McCalla, E. *Accelerated development of high voltage cathodes for Li-ion batteries*. Advanced Energy Materials 2022, 12, 2201704.

S6. Jia, S.; Yao, E.; Peng, R.; Jonderian, A.; Abdolhosseini, M.; McCalla, E. *Chemical speed dating: the impact of 52 dopants in Na-Mn-O cathodes*. Chemistry of Materials 2022, 34, 11047-11061.

S7. Bharti, B.; Kumar, S.; Lee, H.-N.; Kumar, R. Formation of oxygen vacancies and Ti3+ state in TiO2 thin film and enhanced optical properties by air plasma treatment. *Scientific reports* **2016**, *6* (1), 32355.

S8. Huang, C.; Li, R.; Luo, L.; Chen, Y.; Lin, C. The exploration of a CuNb3O8 Li+-storage anode compound. *Materials Technology* **2022**, *37* (8), 814-821.

S9. Kalanur, S. S.; Yoo, I.-H.; Cho, I. S.; Seo, H. Niobium incorporated WO3 nanotriangles: Band edge insights and improved photoelectrochemical water splitting activity. *Ceramics International* **2019**, *45* (7), 8157-8165.

S10. Saha, M.; Ghosh, S.; Paul, S.; Dalal, B.; De, S. K. Nb-Dopant-Induced Tuning of Optical and Electrical Property of Anatase TiO2 Nanocrystals. *ChemistrySelect* **2018**, *3* (23), 6654-6664.

S11. Yun, Y.; Araujo, J. R.; Melaet, G.; Baek, J.; Archanjo, B. S.; Oh, M.; Alivisatos, A. P.; Somorjai, G. A. Activation of tungsten oxide for propane dehydrogenation and its high catalytic activity and selectivity. *Catalysis Letters* **2017**, *147*, 622-632.